Metasurface generated polarization insensitive Fano resonance for high-performance refractive index sensing

HUIGANG LIU,[1,5,†] LU ZHENG,[1,†] PINGZHUN MA,[2] YING ZHONG,[3] BO LIU,[2] XIANZHONG CHEN,[4,6] AND HAITAO LIU[2,7]

[1]Tianjin Key Laboratory of Optoelectronic Sensor and Sensing Network Technology, Department of Microelectronic Engineering, College of Electronic Information and Optical Engineering, Nankai University, Tianjin 300350, China

[2]Tianjin Key Laboratory of Optoelectronic Sensor and Sensing Network Technology, Institute of Modern Optics, College of Electronic Information and Optical Engineering, Nankai University, Tianjin 300350, China

[3]State Key Laboratory of Precision Measurement Technology and Instruments, Tianjin University, Tianjin 300072, China

[4]Institute of Photonics and Quantum Sciences, School of Engineering and Physical Sciences, Heriot-Watt University, Edinburgh EH14 4AS , UK

[5]liuhg@nankai.edu.cn
[6]x.chen@hw.ac.uk
[7]liuht@nankai.edu.cn

[†]These authors contributed equally to this work.

Abstract: A refractive index sensor can provide refractive index measurement and continuously monitor a dynamic process. Plasmonic nanostructure based sensors suffer from severe metal losses in the optical range, leading to the performance degradation. We design and numerically analyze a high-performance refractive index sensor based on the Fano resonance generated by a dielectric metasurface. The figure of merit (FOM) and the maximum quality factor (Q-factor) of the sensor are 721 and 5126, respectively. The maximum modulation depth can exceed 99% and the enhancement factor of the electric field amplitude can reach a high value of about 100. The uniqueness of the proposed sensor is polarization insensitivity. The transmittance spectra for various polarization states of the incident light can perfectly coincide, which is a rare phenomenon in Fano resonance based sensors and can facilitate experimental measurement.

1. Introduction

Metasurfaces are two-dimensional counterparts of metamaterials, which have aroused great interest due to their unprecedented capability in the manipulation of light propagation [1-4]. Benefiting from the advances in micro/nano fabrication technology and extraordinary optical properties of subwavelength structures, considerable efforts have been made on metasurfaces with a wide range of applications including ultra-sensitive bio-chemical sensors, light emitters, slow light, simultaneous detection of the refractive index and the temperature, and so on [5-12]. Metallic nanostructures (e.g., nanorods, nanodiscs) are widely used and explored due to their unique optical properties (e.g., selective field enhancement), leading to the development of early stage refraction index sensing [8, 13]. High-sensitivity sensors based on graphene and hybrid structures were also reported [14-18]. Although the deep-subwavelength concentration of light can be realized, plasmonic nanostructures suffer from the high level of Joules losses at optical frequencies, severely limiting the performance of optical sensors. For example, a refractive index sensor with a sensitivity that can exceed 500 nm/RIU was reported by etching H-shaped aperture structure on the gold film [19], but its figure of merit (FOM) is only 3.8. The full width at half maximum (FWHM) $\Delta\lambda$ of the spectrum is too broad due to the intrinsic Ohmic loss of the metal, dramatically decreasing its FOM. In order to tackle this fundamental challenge, a potential solution is to use high-refractive-index all-dielectric metasurfaces. The advantages of low loss, bandwidth enhancement and isotropic responses in a dielectric metasurface make it a good candidate, providing new opportunities for high-performance sensors [20-22].

Fano resonance originally observed in atomic physics is a kind of asymmetric resonance [23], where the interference between a continuum (or broadband) state and a discrete (or narrowband) state of the structure produces a sharp reflection or transmission spectrum for the light with a given polarization direction. Recently, some new strategies based on dielectric structures have been proposed to achieve high quality factor (Q-factor) Fano resonance [24-26]. Without the hassle of Ohmic losses, the transmission and reflection spectra of dielectric metasurfaces with Fano resonances can be much narrower than those of plasmonic metasurfaces. In addition, the dielectric structures can support both electrical and magnetic dipolar Mie-type resonances[27]. Therefore, they can be used to easily realize magnetic Fano resonance, in which the fundamental resonance mode is a magnetic mode [28, 29]. A composite nanostructure array consisting of silicon nanorings and silicon nanorods were used to design a sensor with a FOM of 103 (due to a 2.8-nm-wide Fano resonance peak) and Q-factor of 483 [30], which cannot be achieved with plasmonic structures. Tunable Fano resonances based on graphene/waveguide hybrid structure were also proposed [31]. However, the generation of Fano resonance usually requires the structure to be asymmetric [32], meaning that the sensor made by this kind of metasurface is sensitive to the polarization of the incident light, which causes the inconvenience for measurement. How to use Fano

resonance generated by a dielectric metasurface to develop a sensor with a property of polarization insensitivity is very challenging.

Here, we propose a high Q-factor refractive index sensor based on the Fano resonance generated by an all-dielectric metasurface. Each unit cell of the designed dielectric metasurface is composed of three identical V-shaped TiO_2 antennas on glass. There are two sharp dips in the transmittance spectrum, at which the Q-factor can reach 5126 with a FOM of 721, the modulation depths ΔT can exceed 99%, and the enhancement factor of the electric field amplitude can reach a high value of about 100, which are superior to previously reported results based on all-dielectric sensors. The transmittance spectrum can be well reproduced and explained with the aid of a Fano model. Furthermore, the sensing properties of the proposed sensor are independent of the polarization state of the incident light, which is a rare phenomenon in Fano resonance sensors and can greatly facilitate experimental measurement.
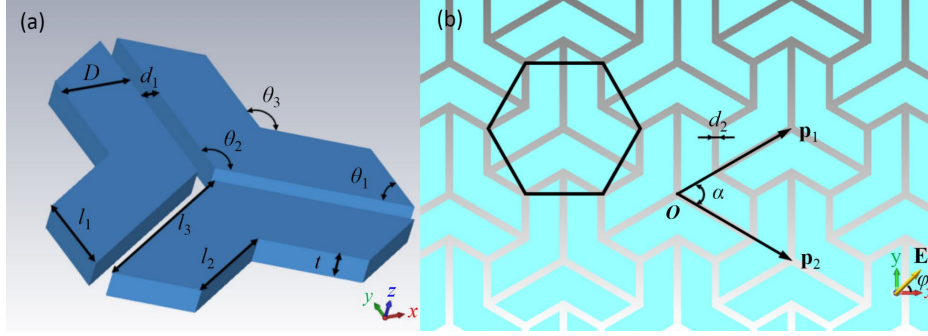
2. Results and discussion

Fig. 1. (a) Schematic of a unit cell of the TiO_2 nanostrucure. (b) Top view of the metasurface, where φ is the angle between the polarization direction of the normally incident light and the x-axis. The structure parameters are $\theta_1=\pi/3$, $\theta_2=\theta_3=2\pi/3$, $D=160$ nm, $d_1=d_2=40$ nm, $t=60$ nm, $l_1=184.75$ nm, $l_2=230.94$ nm, $l_3=415.69$ nm, $\alpha=\pi/3$, $|\mathbf{p}_1|=|\mathbf{p}_2|=692.82$ nm.

The proposed refractive index sensor consists of a TiO_2 nanostructure sitting on a glass substrate. The refractive index of the glass is $n_1=1.5$, and the wavelength-dependent refractive index of TiO_2 is taken from Ref. [33]. The unit cell of the TiO_2 thin film (thickness $t=60$ nm) structure is composed of three identical V-shaped antennas, as shown in Fig. 1(a). Each V-shaped antenna is symmetrical, with $\theta_1=\pi/3$, $\theta_2=\theta_3=2\pi/3$ and $D=160$ nm. There is a gap of $d_1=40$ nm between antennas, and the combined structure has a 3-fold (i.e. 120°) rotational symmetry about the origin point O. Each individual cell is arrayed periodically along the directions of $\mathbf{p}_1$ and $\mathbf{p}_2$ (the angle between them being $\alpha=\pi/3$) to form the structure, as shown in Fig. 1(b). The gap size between adjacent cells is $d_2=d_1=40$ nm, and all the other structural parameters are designed to be $l_1=184.75$ nm, $l_2=230.94$ nm, $l_3=415.69$ nm and $|\mathbf{p}_1|=|\mathbf{p}_2|=692.82$ nm, respectively.
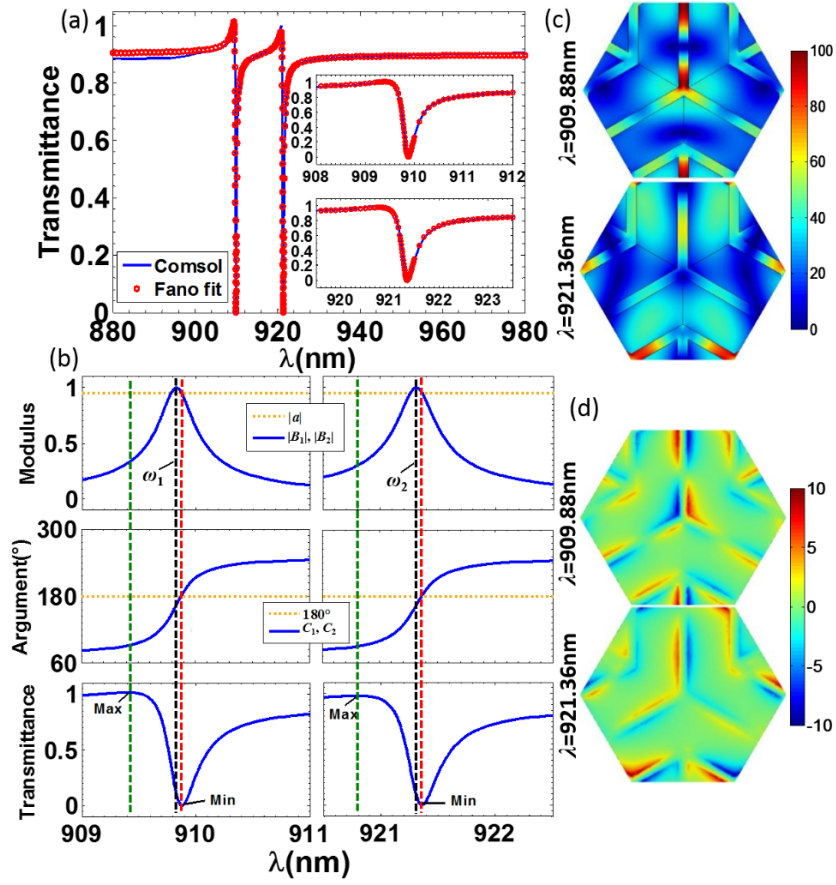
Fig. 2. (a) Transmittance spectrum of the sensor under the illumination of an *x*-polarized plane ve at normal incidence (insets showing the magnified views at the two resonance dips). The surrounding medium is water with a refractive index of 1.333. (b) Explanation of the transmittance spectrum with the Fano model $T(\omega)=|a+B_1+B_2|^2$, where $B_1=b_1/(\omega-\omega_1-i\gamma_1)$ and $B_2=b_2/(\omega-\omega_2-i\gamma_2)$. The first row shows the spectra of the moduli $|a|$ (yellow dotted line), $|B_1|$ and $|B_2|$ (left and right blue curves). The second row shows the spectra of the argument difference $C_1=\arg(B_1)-\arg(a)$ and $C_2=\arg(B_2)-\arg(a)$ (left and right blue curves) and the 180° position (yellow-dotted line). The third row shows the transmittance spectrum predicted by the model. The green, black and red vertical dashed lines mark the wavelengths of the maximum transmittance, the central resonant frequencies ω_1 and ω_2, and the minimum transmittance, respectively. (c) Normalized electric field amplitudes ($|\mathbf{E}|/|\mathbf{E}_0|$, with $\mathbf{E}_0$ denoting the electric vector of the incident plane wave) at the two resonance wavelengths, which are plotted at the central *x-y* plane of the structured TiO$_2$ film. (d) Electric field *z*-component (E_z) at two resonance wavelengths plotted at the *x-y* plane 5 nm above the top surface of the TiO$_2$ film, for which the incident plane wave is normalized to have $E_x=1$ at the top surface of the TiO$_2$ film.

To facilitate simulations, the part surrounded by the black hexagonal wireframe in Fig. 1(b) is chosen as the unit cell of one period. Numerical simulations of the transmittance spectra are carried out with the commercial software COMSOL Multiphysics. The simulated transmittance spectrum of the all-dielectric metasurface under the illumination of an x-polarized [φ=0 as shown in Fig. 1(a)] plane wave at normal incidence is presented in Fig. 2(a) (the blue solid curve). The metasurface is immersed in water with a refractive index of 1.333. Two asymmetrical resonance dips can be observed at the wavelengths λ=909.88 nm and 921.36 nm, respectively. The asymmetrical resonance lineshape is a signature of the Fano resonance. To confirm this point, we will check whether the transmittance spectrum can be reproduced with a Fano model, i.e., $T(\omega)=|a+b/(\omega-\omega_0-i\gamma)|^2$, where a and b are complex numbers in general, ω and ω_0 are the scanned and central resonant angular frequencies, respectively, and γ represents the damping rate of the resonance [34, 35]. Here the term a and the term $b/(\omega-\omega_0-i\gamma)$ represent a continuous mode and a discrete resonant mode, respectively. For the time-dependent factor $\exp(i\omega t)$ adopted in the Comsol software, there is γ>0 due to the energy leakage of the resonant mode with time [36]. Since there are two resonance dips in the transmittance spectrum, $T(\omega)=|a+b_1/(\omega-\omega_1-i\gamma_1)+b_2/(\omega-\omega_2-i\gamma_2)|^2$ is used for reproducing the transmittance spectrum. The obtained model parameters are a=0.5898−0.7433i, b_1=(3.0846+1.1366i)×10^{11} s^{-1}, $2\pi c/\omega_1$=909.83 nm, $2\pi c/\gamma_1$=5.7195 × 10^6 nm, b_2=(3.3270+1.2436i)×10^{11} s^{-1}, $2\pi c/\omega_2$=921.31 nm, and $2\pi c/\gamma_2$=5.2918×10^6 nm, respectively. As shown in Fig. 2(a), the prediction of the Fano model (red circles) agrees well with the full-wave numerical results (blue solid curve) especially near the resonance dips, which confirms the Fano-resonance essence of the transmittance spectrum.

By virtue of the model, it is also possible to achieve an insight into the formation of the asymmetrical lineshape of the Fano resonance. For convenience, we denote B_1=$b_1/(\omega-\omega_1-i\gamma_1)$, B_2=$b_2/(\omega-\omega_2-i\gamma_2)$, C_1=arg(B_1)−arg(a) and C_2=arg(B_2)−arg(a). Figure 2(b) shows that with the increase of the wavelength (or decrease of frequency) that goes across the central resonant frequency, $|B_1|$ and $|B_2|$ exhibit a symmetrical Lorentzian resonance lineshape along with an increase of C_1 and C_2 by about 180°, which can be easily understood in view of 0<γ_1<<ω_1 and 0<γ_2<<ω_2. Then the almost-zero resonance dip of transmittance T is formed by a destructive interference between the continuous mode (a) and resonant modes (B_1 and B_2), i.e. $|B_1|$=$|a|$ with C_1=180°, and $|B_2|$=$|a|$ with C_2=180°, which occurs in the region quite close to the central resonant frequencies ω_1 and ω_2. In contrast, the almost-unity transmittance is formed by an approximate constructive interference between the continuous mode and resonant modes with a moderate phase difference (C_1 and C_2) far from 180° and a moderate value of $|B_1|$ and $|B_2|$.

With the above model, the Q-factors can be estimated as Q=$\omega_1/(2\gamma_1)$ and $\omega_2/(2\gamma_2)$, which can reach 3143 and 2872 at the two dips, respectively. With the other definition of the Q-factor, Q=$\lambda_{res}/\Delta\lambda$, where λ_{res} is the resonance wavelength at the transmittance dip and $\Delta\lambda$ is the full width at the half maximum (FWHM), one can obtain Q=3148 and 2870

(corresponding to $\Delta\lambda$=0.289 and 0.321 nm) at the two transmittance dips, quite close to the results of the Fano model. The modulation depths ΔT, which are defined as the differences of transmittance between the Fano peaks and the Fano dips $T_{peak}-T_{dip}$, are 99.81% and 99.79% at the two resonances, respectively. These characteristics are superior to many other refractive index sensors of all-dielectric metasurfaces [37].

Figure 2(c) shows the normalized electric-field amplitude distribution at the two wavelengths of transmittance dips. It can be seen that the enhancement factor of the electric field amplitude at both resonances can reach a high value of about 100 (in the groove), although their field distributions are different. This magnitude of enhancement factor may be common to plasmonic nanostructures, but it is unusual to all-dielectric metasurfaces. For some applications, such as nonlinear optics and enhanced Raman scattering [38, 39], it is desirable to have strong field enhancement and light localization in the gaps. To further elucidate the presence of the Fano resonance, the distributions of z-component E_z of electric field at the two resonance dips are plotted in Fig. 2(d). One can see the strong E_z field near the grooves and the anti-phased oscillations of displacement currents on both sides of the grooves, which is also a feature of the Fano resonance [24, 40].
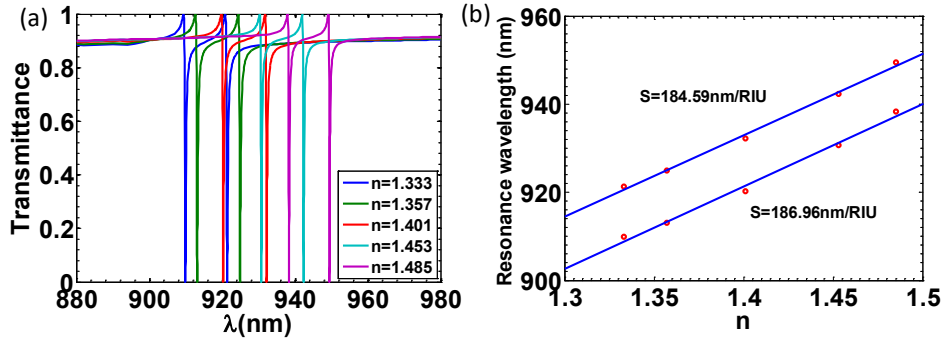

Fig. 3. (a) Transmittance spectra of the proposed metasurface refractive-index sensor covered by liquids with different refractive indices n. (b) Shifts of the resonance wavelengths at the two Fano transmittance dips as a function of the surrounding refractive index.

The overall performance of refractive-index sensors can be evaluated by the FOM, which is defined as FOM=$S/\Delta\lambda$, where S is the sensitivity defined as the resonance wavelength shift per refractive-index-unit change of the surrounding medium. To assess the performance of the sensor, we consider various liquid substances with different refractive indices, such as water with n=1.333, ethanol (C_2H_5OH) with n=1.357, pentanol ($C_5H_{11}OH$) with n=1.401, carbon tetrachloride (CCl_4) with n=1.453, and benzene (C_6H_6) with n=1.485. The five liquids are chosen in view that they have a large refractive index difference. Figure 3(a) shows the transmittance spectra of the metasurface when immersed in the different liquids. With the increase of the refractive index, the resonance wavelengths exhibit a red shift, along with a

decrease of $\Delta\lambda$ and an increase of Q-factor. The Q-factor can reach a maximum of 5126 with $\Delta\lambda$=0.185 nm, at the second Fano dip of transmittance for n=1.485. The modulation depth ΔT is larger than 99% for all the considered liquids. From the line fit in Fig. 3(b), the sensitivity at the two resonances are estimated to be S=186.96 nm/RIU and 184.59 nm/RIU, respectively. Despite the moderate values of S, the low values of $\Delta\lambda$ (0.261 nm and 0.256 nm at the resonance dips) result in high values of the FOM (716 and 721), which are superior to the previously reported values that are usually less than 300 [37].

With the rapid development of nanofabrication technology, the designed V-shaped antennas can be fabricated in many research groups. For example, V-shaped antennas [41] and V-shaped slits [42] have been fabricated based on the electron beam lithography (EBL) and focused ion beam (FIB) milling, respectively. To analyze the effect of the fabrication error on the sensing performance, we consider a change of the gap size (d_1=d_2) by ±5nm with other geometrical sizes unchanged. As shown in Table 1 (with a surrounding medium of water), the increase of the gap size here leads to a slight change of the sensitivity, a slight decrease of the Q factor and the FOM value, and a small blue shift of the Fano resonance dips.

Table 1. Comparison of Sensing Performances for Different Gap Sizes.

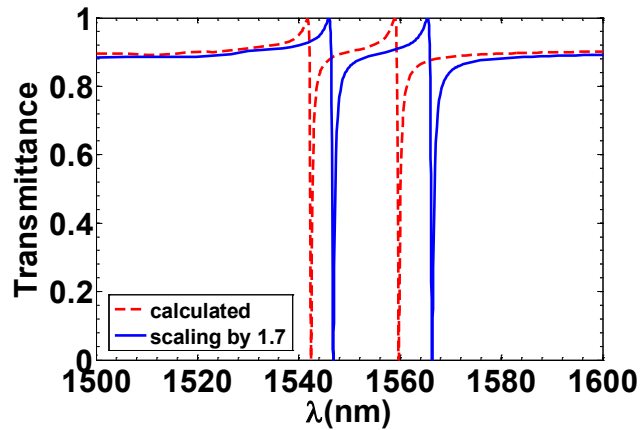| Gap size (nm)	35		40		45	
Resonance dip	Dip 1	Dip 2	Dip 1	Dip 2	Dip 1	Dip 2
Dip Wavelength (nm)	913.86	925.22	909.88	921.36	906.56	917.8
Sensitivity (nm/RIU)	189.54	183.63	186.96	184.59	182.76	185.33
Q factor	3181	3190	3143	2872	3103	2561
FOM	778	811	716	721	682	647

Fig. 4 Transmittance spectrum of the new refractive-index sensor with all geometrical sizes scaled up by a factor of 1.7. The results obtained with the calculation and the wavelength scaling are shown with red dashed and blue solid curves, respectively.

Although the resonance wavelengths of the proposed sensor range from 0.88 to 0.98 μm, they can be readily tuned to other wavelength ranges such as the communication or visible wavelengths just by changing all geometrical parameters with the wavelength. For nondispersive materials, the scaling law of Maxwell's equations ensures that the transmittance spectra are unchanged if all the geometrical parameters are scaled proportionally to the wavelength. Thus the weak material dispersion of the proposed dielectric metasurface can ensure an approximate invariance of the transmittance spectra (and the resultant sensing performances) when scaling to other wavelength ranges.

To confirm this point, we make further calculations at communication wavelengths after scaling up all the geometrical sizes by a factor of 1.7. Here we consider the actual material dispersion of TiO_2 [33] and neglect the weak dispersion of the glass substrate and of the surrounding medium of water. For instance, the refractive index of TiO_2 changes from 2.497 at wavelength 909.88 nm to 2.453 at wavelength 1542.42 nm. As shown in Fig. 4, the transmittance spectrum at communication wavelengths (red dashed curve) is quite close to the curve in Fig. 2(a) with all wavelengths multiplied by 1.7 (blue curve), which can be understood in view of the scaling law of Maxwell's equations and the weak dispersion of TiO_2. Table 2 shows that scaling to communication wavelengths even exhibits better sensing performances.

Table 2. Comparison between the Proposed Original Structure and the New Scaled up Structure.

Structure	Original Structure		New Structure	
Resonance Dip	Dip 1	Dip 2	Dip 1	Dip 2
Dip Wavelength (nm)	909.88	921.36	1542.42	1559.73
Sensitivity (nm/RIU)	186.96	184.59	311.7	313.62
Q factor	3143	2872	3787	3371
FOM	716	721	854	852

Symmetry-breaking structures are typically used to produce Fano resonance, which usually causes the transmittance or reflectance spectra to be sensitive to the polarization state of the incident light and leads to inconvenience for the measurement. The 90° (i.e. 4-fold) rotational symmetry along with a bilateral mirror symmetry is routinely used in the literatures to ensure the polarization independence [43-45]. However, as shown here, the proposed metasurface exhibits polarization-independent characteristics despite its breaking of the 90° rotational symmetry about the origin point O [see Fig. 1(b)]. Figure 5(a) shows the transmittance spectra of the metasurface immersed in water when the polarization states of

the incident light are right-handed circular polarization (RCP, blue circles), *x*-polarization ($\varphi=0$, red-solid curve) and *y*-polarization ($\varphi=\pi/2$, yellow asterisks), respectively. It is seen that the transmittance spectra for the three incidence polarizations coincide perfectly, showing the unique property of polarization insensitivity of the structure. To further confirm this point, we calculate the transmittance spectra with the polarization angle φ varying continuously from 0 to $\pi/2$, as shown in Fig. 5(b). It is seen that the transmittance spectra hardly changes with φ, indicating that the refractive index sensor is insensitive to the polarization direction of the incident light. The distributions of normalized electric-field amplitude at the two resonance dips obtained for several polarization states are provided in Fig. 5(c). One can see that although the transmittances for different φ take almost identical dip values at the same resonance wavelengths [as shown by the magnified views in Fig. 5(b)], the corresponding field distributions are not similar due to the breaking of the 4-fold rotational symmetry.
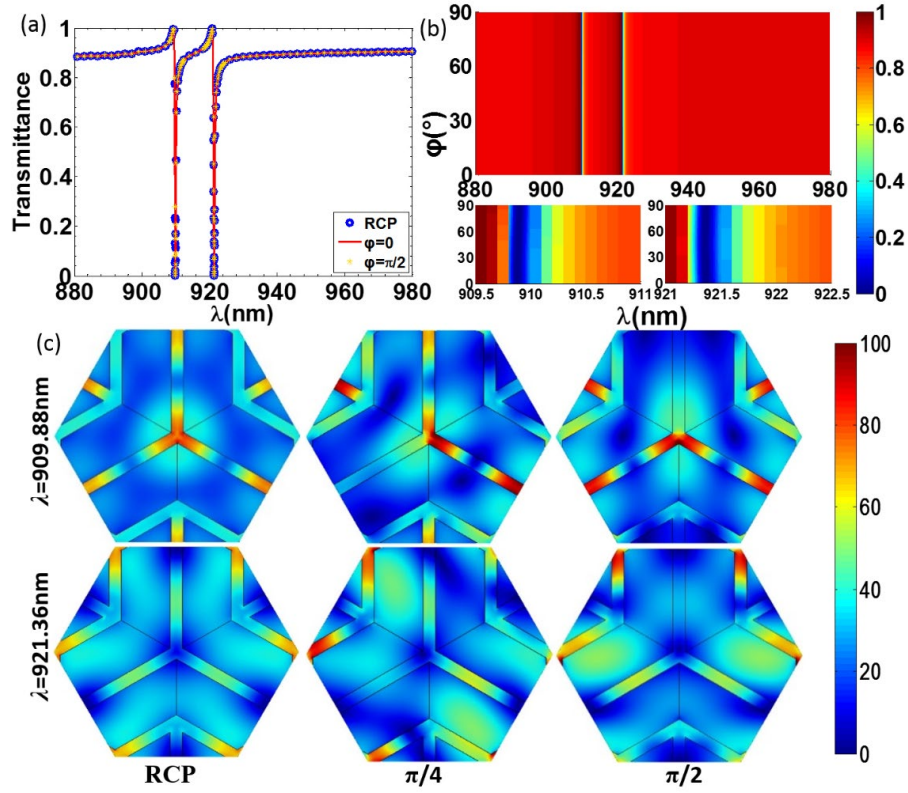

Fig. 5. (a) Transmittance spectra for a normally incident plane wave of RCP (blue circles), *x*-polarization ($\varphi=0$, red solid curve) and *y*-polarization ($\varphi=\pi/2$, yellow asterisks) with a surrounding medium of water (refractive index *n*=1.333). (b) Transmittance obtained for different polarization angles φ and wavelengths. The two figures below provide magnified

To unveil the mechanism why the transmittance is insensitive to the incidence polarization, next we will theoretically demonstrate that the 120° (i.e. 3-fold) rotational symmetry about the origin point O along with the mirror symmetry about $x=0$ of the proposed structure must ensure the polarization independence when the light impinges on the device at normal incidence. We first consider the case that the normally incident plane wave is linearly polarized along the y direction, i.e. with an electric vector $\mathbf{E}_{0,i}=c_i\mathbf{y}$ with c_i being a complex amplitude coefficient and $\mathbf{y}$ being the unit vector along the y-direction. Then according to the symmetry theorem of the Maxwell's equations [46], the simultaneous mirror symmetries of the structure and of the $\mathbf{E}_{0,i}$ about the $x=0$ plane will result in the same mirror symmetry of the zeroth-order transmitted plane wave, i.e. with an electric vector $\mathbf{E}_{0,t}=c_it\mathbf{y}=t\mathbf{E}_{0,i}$, where $t=t(\lambda)$ is a complex transmission coefficient. Then the zeroth-order transmittance can be expressed as

$$T_0(\lambda) = \frac{\left|\mathbf{S}_{0,t}\right|}{\left|\mathbf{S}_{0,i}\right|} = \frac{\frac{n_t}{2\eta_0}\mathbf{E}_{0,t}\bullet\mathbf{E}_{0,t}^{*}}{\frac{n_i}{2\eta_0}\mathbf{E}_{0,i}\bullet\mathbf{E}_{0,i}^{*}} = \frac{n_t}{n_i}\left|t(\lambda)\right|^2 \ , \tag{1}$$

where $\mathbf{S}_{0,i}$ and $\mathbf{S}_{0,t}$ are the Poynting vectors of the incident and zeroth-order transmitted plane waves, respectively, η_0 is the wave impedance in vacuum, and n_i and n_t are the refractive indices of the incidence and transmittance half-spaces, respectively. Then we consider the general case of a normally-incident plane wave with an arbitrary polarization, i.e. $\mathbf{E}_i=c_{i,x}\mathbf{x}+c_{i,y}\mathbf{y}$, with $\mathbf{x}$ and $\mathbf{y}$ being unit vectors along the x- and y-directions, and $c_{i,x}$ and $c_{i,y}$ being the corresponding complex amplitude coefficients. With ($\mathbf{x},\mathbf{y}$) projected upon a new set of non-orthogonal vector basis ($\mathbf{a}_1,\mathbf{a}_2$), where we choose $\mathbf{a}_1=\mathbf{y}$ and $\mathbf{a}_2=\mathbf{x}\cos30°-\mathbf{y}\sin30°$ being the unit vector along the $\mathbf{p}_2$ direction as shown in Fig. 1(b), $\mathbf{E}_i$ can be instead expressed as $\mathbf{E}_i=c_{i,1}\mathbf{a}_1+c_{i,2}\mathbf{a}_2$. Because the structure does not change when it rotates 120° relative to the origin point O, the electric vector of the zeroth-order transmitted plane wave should be $\mathbf{E}_t=c_{i,1}t\mathbf{a}_1$ or $c_{i,2}t\mathbf{a}_2$ for $\mathbf{E}_i=c_{i,1}\mathbf{a}_1$ or $c_{i,2}\mathbf{a}_2$, respectively. According to the linear superposition principle of Maxwell's equations, we finally obtain $\mathbf{E}_t=c_{i,1}t\mathbf{a}_1+c_{i,2}t\mathbf{a}_2=t\mathbf{E}_i$ for $\mathbf{E}_i=c_{i,1}\mathbf{a}_1+c_{i,2}\mathbf{a}_2$, and the resultant zeroth-order transmittance is

$$T(\lambda) = \frac{\frac{n_t}{2\eta_0}\mathbf{E}_t\bullet\mathbf{E}_t^{*}}{\frac{n_i}{2\eta_0}\mathbf{E}_i\bullet\mathbf{E}_i^{*}} = \frac{n_t}{n_i}\left|t(\lambda)\right|^2 , \tag{2}$$

From Eqs. (1) and (2), one can derive $T(\lambda)=T_0(\lambda)$ which is independent of the coefficients $c_{i,1}$ and $c_{i,2}$, namely, the transmittance for any polarization state of incidence is the same. The above theoretical demonstration provides a new strategy for the design of polarization-independent structures, which employs the 3-fold rotational symmetry instead of the 4-fold rotational symmetry routinely used in literatures.

Table 3 shows the comparison of our proposed sensor with other reported refractive index sensors in terms of material, structure, sensitivity, Q, FOM and polarization sensitivity. We can see that most of the existing refractive index sensors are sensitive to the polarization state of the incident light. Among various polarization-insensitive sensors, the sensor proposed in this paper has the largest FOM, which is a very important parameter to characterize the overall sensing performance.

Table 3. Comparison of the Existing Refractive Index Sensors in Literatures and Our Work.

Reference (year)	Material	Structure	Sensitivity in Unit nm/RIU (Method)	Q factor (Method)	FOM (Method)	Polarization Sensitivity
5 (2011)	Au	Double Split Nano-ring Cavity	1218 (Simulation)	-	8.6 (Simulation)	Sensitive
6 (2013)	Au	Split-ring Resonators / Disk	282 (Experiment)	-	4 (Experiment)	Sensitive
8 (2009)	Au	Nanorod	32000 (Estimation)	-	330 (Estimation)	Sensitive
19 (2010)	Au	H-shaped Aperture	588 (Experiment)	-	3.8 (Experiment)	Sensitive
24 (2014)	Si	Split-bar	525 (Simulation)	800 (Simulation)	260 (Simulation)	Sensitive
26 (2018)	Si	Nanobar Pairs	370 (Simulation)	10000 (Simulation)	2846 (Simulation)	Sensitive
30 (2014)	Si	Nanoring and Nanorods	289 (Experiment)	483 (Experiment)	37 (Experiment)	Sensitive
37 (2018)	Si	Glasses-shaped	433.05 (Simulation)	412.6 (Simulation)	116.7 (Simulation)	Sensitive
42 (2018)	Si	Split Ring	452 (Simulation)	133 (Simulation)	56.5 (Simulation)	Sensitive
12 (2017)	Si	Four Holes in Nanoblock Unit	306.71 (Simulation)	-	10.09 (Simulation)	Insensitive
13 (2010)	Au	Disk	400 (Experiment)	-	87 (Experiment)	Insensitive
22 (2019)	a-Si	Cylinder	350 (Simulation) 323 (Experiment)	-	219 (Simulation) 5.4 (Experiment)	Insensitive
our paper	TiO$_2$	V-shaped	186.96 (Simulation)	5126 (Simulation)	721 (Simulation)	Insensitive

3. Conclusion

In summary, we propose an all-dielectric metasurface refractive-index sensor based on Fano resonance with superior performance compared to the recently reported devices. The transmittance spectrum exhibits two Fano resonance dips, at which the Q-factor and FOM reach high values up to 5126 and 721, respectively, along with a modulation depth greater than 99%, a sensitivity of 186.96 nm/RIU and an electric-field amplitude enhancement of about 100 times. The asymmetrical lineshape of the transmittance spectrum at resonance can be well reproduced with the use of a Fano model, which confirms the Fano-resonance essence and further provides some insight into the formation of the asymmetrical lineshape. In addition, despite its breaking of the 4-fold rotational symmetry, the proposed sensor exhibits Fano resonance that does not change with the polarization state of the incident light, which brings great convenience to the measurement. We theoretically demonstrate that the polarization independence of the Fano resonance is due to the 3-fold rotational symmetry along with one mirror symmetry of the structure, providing new design strategies for the polarization-independent devices and enriching the relevant physics of Fano resonance.

Funding

REFERENCES

1. D. Wen, F. Yue, W. Liu, S. Chen, and X. Chen, "Geometric metasurfaces for ultrathin optical devices," Adv. Opt. Mater. **6**, 1800348 (2018).

2. D. Hu, X. Wang, S. Feng, J. Ye, W. Sun, Q. Kan, P. J. Klar, and Y. Zhang, "Ultrathin terahertz planar elements," Adv. Opt. Mater. **1**, 186-191 (2013).

3. G. Zheng, H. Mühlenbernd, M. Kenney, G. Li, T. Zentgraf, and S. Zhang, "Metasurface holograms reaching 80% efficiency," Nat. Nanotechnol. **10**, 308 (2015).

4. X. Yin, T. Steinle, L. Huang, T. Taubner, M. Wuttig, T. Zentgraf, and H. Giessen, "Beam switching and bifocal zoom lensing using active plasmonic metasurfaces," Light-Sci. Appl. **6**, e17016 (2017).

5. S. Liu, Z. Yang, R. Liu, and X. Li, "High sensitivity localized surface plasmon resonance sensing using a double split nano-ring cavity," J. Phys. Chem. C **115**, 24469-24477 (2011).

6. Q. Zhang, X. Wen, G. Li, Q. Ruan, J. Wang, and Q. Xiong, "Multiple magnetic mode-based Fano resonance in split-ring resonator/disk nanocavities," ACS Nano **7**, 11071-11078 (2013).

7. A. Ahmadi and H. Mosallaei, "Physical configuration and performance modeling of all-dielectric metamaterials," Phy. Rev. B **77**, 045104 (2008).

8. A. V. Kabashin, P. Evans, S. Pastkovsky, W. Hendren, G. A. Wurtz, R. Atkinson, R. Pollard, V. A. Podolskiy, and A. V. Zayats, "Plasmonic nanorod metamaterials for biosensing," Nat. Mater. **8**, 867-871 (2009).

9.   Q. Zhao, J. Zhou, F. Zhang, and D. Lippens, "Mie resonance-based dielectric metamaterials," Mater. Today **12**, 60-69 (2009).

10.   M. Siltanen, S. Leivo, P. Voima, M. Kauranen, P. Karvinen, P. Vahimaa, and M. Kuittinen, "Strong enhancement of second-harmonic generation in all-dielectric resonant waveguide grating," Appl. Phys. Lett. **91**, 111109 (2007).

11.   C. Argyropoulos, "Enhanced transmission modulation based on dielectric metasurfaces loaded with graphene," Opt. Express **23**, 23787-23797 (2015).

12.   J. Hu, T. Lang, and G. Shi, "Simultaneous measurement of refractive index and temperature based on all-dielectric metasurface, " Opt. Express **25**, 15241-15251 (2017).

13.   N. Liu, M. Mesch, T. Weiss, M. Hentschel, and H. Giessen, "Infrared perfect absorber and its application as plasmonic sensor," Nano Lett. **10**, 2342-2348 (2010).

14.   B. Ruan, Q. You, J. Zhu, L. Wu, J. Guo, X. Dai, and Y. Xiang, "Fano resonance in double waveguides with graphene for ultrasensitive biosensor," Opt. Express **26**, 16884-16892 (2018).

15.   L. Wu, J. Guo, H. Xu, X. Dai, and Y. Xiang, "Ultrasensitive biosensors based on long-range surface plasmon polarition and dielectric waveguide modes," Photon. Res. **4**, 262-266 (2016).

16.   L. Wu, Y. Jia, L. Jiang, J. Guo, X. Dai, Y. Xiang, and D. Fan, "Sensitivity improved SPR biosensor based on the MoS_2/graphene-aluminum hybrid structure," J. Lightwave Technol. **35**, 82-87 (2017).

17.   B. Ruan, J. Guo, L. Wu, J. Zhu, Q. You, X. Dai, and Y. Xiang, "Ultrasensitive terahertz biosensors based on Fano resonance of a graphene/waveguide," Sensors. **17**, 1924 (2017).

18.   L. Wu, J. Guo, Q. Wang, S. Lu, X. Dai, Y. Xiang, and D. Fan, "Sensitivity enhancement by using few-layer black phosphorus-graphene/TMDCs heterostructure in surface plasmon resonance biochemical sensor," Sensors and Actuators B: Chemical. **249**, 542-548 (2017).

19.   N. Liu, T. Weiss, M. Mesch, L. Langguth, U. Eigenthaler, M. Hirscher, C. Sonnichsen, and H. Giessen, "Planar metamaterial analogue of electromagnetically induced transparency for plasmonic sensing," Nano Lett. **10**, 1103-1107 (2010).

20.   A. I. Kuznetsov, A. E. Miroshnichenko, M. L. Brongersma, Y. S. Kivshar, and B. Luk'yanchuk, "Optically resonant dielectric nanostructures," Science **354**, aag2472 (2016).

21.   D. G. Baranov, D. A. Zuev, S. I. Lepeshov, O. V. Kotov, A. E. Krasnok, A. B. Evlyukhin, and B. N. Chichkov, "All-dielectric nanophotonics: the quest for better materials and fabrication techniques," Optica **4**, 814-825 (2017).

22.   A. J. Ollanik, I. O. Oguntoye, G. Z. Hartfield, and M. D. Escarra, "Higly sensitive affordable, and adaptable refractive index sensing with silicon-based dielectric metasurfaces," Adv. Mater. Technol. **4**, 1800567 (2019).

23.   U. Fano, "Effects of configuration interaction on intensities and phase shifts," Phys. Rev. **124**, 1866-1878 (1961).

24.   J. Zhang, W. Liu, Z. Zhu, X. Yuan, and S. Qin, "Strong field enhancement and light-matter interactions with all-dielectric metamaterials based on split bar resonators," Opt. Express **22**, 30889-30898 (2014).

25. Y. Liu, Y. Luo, X. Jin, X. Zhou, K. Song, and X. Zhao, "High-Q Fano resonances in asymmetric and symmetric all-dielectric metasurfaces," Plasmonics **12**, 1431-1438 (2016).

26. Y. Zhang, W. Liu, Z. Li, Z. Li, H. Cheng, S. Chen, and J. Tian, "High-quality-factor multiple Fano resonances for refractive index sensing," Opt. Lett. **43**, 1842-1845 (2018).

27. J. C. Ginn, I. Brener, D. W. Peters, J. R. Wendt, J. O. Stevens, P. F. Hines, L. I. Basilio, L. K. Warne, J. F. Ihlefeld, P. G. Clem, and M. B. Sinclair, "Realizing optical magnetism from dielectric metamaterials," Phys. Rev. Lett. **108**, 097402 (2012).

28. B. Hopkins, D. S. Filonov, A. E. Miroshnichenko, F. Monticone, A. Alù, and Y. S. Kivshar, "Interplay of magnetic responses in all-dielectric oligomers to realize magnetic Fano resonances," ACS Photonics **2**, 724-729 (2015).

29. K. E. Chong, B. Hopkins, I. Staude, A. E. Miroshnichenko, J. Dominguez, M. Decker, D. N. Neshev, I. Brener, and Y. S. Kivshar, "Observation of Fano resonances in all-dielectric nanoparticle oligomers," Small **10**, 1985-1990 (2014).

30. Y. Yang, Kravchenko, II, D. P. Briggs, and J. Valentine, "All-dielectric metasurface analogue of electromagnetically induced transparency," Nat. Commun. **5**, 5753 (2014).

31. J. Guo, L. Jiang, X. Dai and Y. Xiang, "Tunable Fano resonances of a graphene/waveguide hybrid structure at mid-infrared wavelength, " Opt. Express **24**, 4740-4748 (2016).

32. A. E. Miroshnichenko, S. Flach, and Y. S. Kivshar, "Fano resonances in nanoscale structures," Rev. Mod. Phys. **82**, 2257-2298 (2010).

33. J. R. DeVore, "Refractive indices of rutile and sphalerite," J. Opt. Soc. Am. **41**, 416-419 (1951).

34. C. Wu, N. Arju, G. Kelp, J. A. Fan, J. Dominguez, E. Gonzales, E. Tutuc, I. Brener, and G. Shvets, "Spectrally selective chiral silicon metasurfaces based on infrared Fano resonances," Nat. Commun. **5**, 3892 (2014).

35. D. Tang and W. Ding, "Fano resonance by symmetry breaking stub in a metal-dielectric-metal waveguide," Chin. Phys. Lett. **31**, 057301 (2014).

36. P. Lalanne, W. Yan, K. Vynck, C. Sauvan, and J.-P. Hugonin, "Light interaction with photonic and plasmonic resonances," Laser Photon. Rev. **12**, 1700113 (2018).

37. J. Hu, T. Lang, Z. Hong, C. Shen, and G. Shi, "Comparison of electromagnetically induced transparency performance in metallic and all-dielectric metamaterials," J. Lightwave Technol. **36**, 2083-2093 (2018).

38. G. McNay, D. Eustace, W. E. Smith, K. Faulds, and D. Graham, "Surface-enhanced Raman scattering (SERS) and surface-enhanced resonance Raman scattering (SERRS): a review of applications," Appl. Spectrosc. **65**, 825-837 (2011).

39. M. Kauranen and A. V. Zayats, "Nonlinear plasmonics," Nat. Photonics **6**, 737 (2012).

40. G. Liu, X. Zhai, L. Wang, Q. Lin, S. Xia, X. Luo, and C. Zhao, "A high-performance refractive index sensor based on Fano resonance in Si split-ring metasurface," Plasmonics **13**, 15-19 (2018).

41. E. Karimi, S. A Schulz, I. D. Leon, H. Qassim, J. Upham and R. W. Boyd, "Generating optical orbital angular momentum at visible wavelengths using a plasmonic metasurface," Light-Sci. Appl. **3**, e167 (2014)

42. X. Ni, A. V. Kildishev and V. M. Shalaev, "Metasurface holograms for visible light," Nat. Commun. **4**, 2807 (2013).

43. I. A. I. Al-Naib, C. Jansen, N. Born, and M. Koch, "Polarization and angle independent terahertz metamaterials with high Q-factors," Appl. Phys. Lett. **98**, 091107 (2011).

44. C. Hua, C. Shuqi, Y. Haifang, L. Junjie, A. Xin, G. Changzhi, and T. Jianguo, "A polarization insensitive and wide-angle dual-band nearly perfect absorber in the infrared regime," J. Opt. **14**, 085102 (2012).

45. L. Wu, Z. Yang, M. Zhao, Y. Zheng, J. a. Duan, and X. Yuan, "Polarization-insensitive resonances with high quality-factors in meta-molecule metamaterials," Opt. Express **22**, 14588-14593 (2014).

46. C. Vassallo, *Optical Waveguide Concepts* (Elsevier, 1991).